



A two parameter model to simulate thermal infrared directional effects for remote sensing applications



C. Duffour^a, J.-P. Lagouarde^{a,*}, J.-L. Roujean^b

^a INRA, UMR 1391 ISPA, F-33140 Villenave d'Ornon, France

^b Météo France CNRM-GAME, F-31057 Toulouse, France

ARTICLE INFO

Article history:

Received 15 October 2015

Received in revised form 5 July 2016

Accepted 8 August 2016

Available online xxx

Keywords:

Directional anisotropy

Land surface temperature

Thermal infrared (TIR) remote sensing

Parametric model

SCOPE

ABSTRACT

Measurements of land surface temperature (LST) performed in the thermal infrared (TIR) domain are prone to strong directional anisotropy. Instead of detailed analytical physical TIR models requiring too much input information and computational capacities, simplified parametric approaches capable to mimic and correct with precision the angular effects on LST will be deemed suitable for practical satellite applications. In this study, we present a simple two parameters model, so-called RL (Roujean-Lagouarde), which shows capabilities to properly depict the directional signatures of both urban and vegetation targets within an accuracy better than 1 °C. This latter value is the RMSE (root mean square error) obtained as the best adjustment of the RL model against in situ datasets. Then the RL approach was compared to a synthetic dataset generated by the model Soil Canopy Observation, Photochemistry and Energy fluxes (SCOPE) in which large variability in meteorological scenarios, canopy structure and water status conditions was accounted for. Results indicate RMSE ≤ 0.6 °C which is a very hopeful result. Besides, the RL model performs even better than the popular parametric model of Vinnikov that encompasses two unknowns. The ability of RL model to better reproduce the hotspot phenomenon explains this feature.

The RL model appears as a potential candidate for future operational processing chains of TIR satellite data because it fulfills the requirements of both simple analytical formulation and limited number of input parameters. Efforts nevertheless remain to be done on inversion methodologies.

© 2016 Elsevier Inc. All rights reserved.

1. Introduction

Thermal infrared (TIR) measurements are widely used to retrieve land surface temperature (LST) which is a useful proxy to derive surface fluxes, especially evapotranspiration. However these measurements are prone to strong directional anisotropic effects. These can be defined as the difference between off-nadir and nadir temperatures. Such difference can reach up to 15 °C according to various authors (Kimes and Kirchner, 1983; Lagouarde et al., 2014).

Efforts have been made in the past to model the TIR radiation anisotropy in following geometric, radiative transfer, 3-dimensional and parametric approaches. A review can be found in Verhoef et al. (2007). Duffour et al. (2015b) recently demonstrated the ability of the Soil-Vegetation-Atmosphere Transfer (SVAT) model SCOPE (Van der Tol et al., 2009) which combines a detailed description of both physical and physiological processes to simulate TIR directional anisotropy. Actually, TIR data processing is in need of simple models for several purposes. First reason is to be able to correct TIR remote sensing data from directional effects using a fast and computationally efficient method. For such, one

must only consider algorithms (i) requiring a few input data and (ii) being analytically interpretable for ease of implementation into operational satellite data processing chains. Secondly, simple models are very helpful for a rapid assessment of the impact of the angular sampling, which is particularly relevant for the design of experimental campaigns with the concern of optimizing the instrumental protocol.

Simple parametric models are attractive in many ways. Because of their limited number of input parameters, the inversion procedure is more certain. Another asset is that they can be relevant at any spatial scale, in particular when linearity of the model is possible. Moreover, parametric models may be more robust to measurement noise compared to deterministic models which are affected by the cumulative uncertainties of the large input datasets they require. Parametric models can be totally empirical or based on physical assumptions. Although parametric models are widely used to correct optical BRDF (Bi-directional Reflectance Distribution Function), such an approach has not yet been developed so far to process and analyze TIR data. One limitation however would be the prescription of a priori values for the input parameters, unless their physical meaning may be well determined through field experiments for instance.

When approaching TIR satellite measurements through modeling, a primary assumption is that any sensor pixel is the sum of dissociated elementary photometric quantities. These latter can be further modeled

* Corresponding author.

E-mail address: lagouarde@bordeaux.inra.fr (J.-P. Lagouarde).

as a linear combination of mathematical functions sketched by kernels being trigonometric functions of the geometry of observation. In the optical domain, the kernel approach has been successful to mimic the BRDF (Wanner et al., 1995; Jupp, 2000; Bréon et al., 2002; Vermote et al., 2009). In the TIR domain, it has been applied to simulate the directional anisotropy of surface emissivity (Snyder and Wan, 1998; Su et al., 2002). In order to model the radiation anisotropy on TIR signal and further on temperature from geostationary satellites observations, Vinnikov et al. (2012) developed a parametric model of TIR anisotropy based on only two kernels.

Generally speaking, the solution to the inverse problem may be obtained by generating first Look Up Tables (LUTs) issued from simulations of a sophisticated TIR model, at the cost of some training for initiate some machine learning. Even so, and to our knowledge, this possibility has not been evaluated yet in the TIR domain. However, in the context of remote sensing applications, the robustness of the solution is indeed a real concern in order to comply with possibly noisy and sparse observations.

This justifies for another approach here consisting in the derivation of analytical expressions departing from simplified assumptions on the physics. For instance Roujean (2000) and Bréon et al. (2002) have proposed two models of hot spot simplifying the radiative transfer processes inside canopies for optical remote sensing applications. In the TIR, Lagouarde and Irvine (2008) adapted the Roujean (2000) model to derive a parametric expression of directional anisotropy requiring two parameters only to be known or adjusted. A first favorable test was obtained against experimental measurements acquired over an urban canopy. The simplicity of the model makes it very attractive to characterize the directional anisotropy.

Nevertheless it still requires to be extensively evaluated. Such is the goal of this paper. In a first section, the model will be described and its ability to simulate DA over vegetation demonstrated. The scarcity of available experimental DA datasets providing both azimuth and zenith angular information led us to assess the reliability of the model in a second step by testing it against a synthetic dataset generated by a deterministic model, SCOPE. Here, SCOPE is used as a data generator, for a large range of realistic conditions that can be met: structure of the canopy, water status, meteorological forcing. A third section finally proposes a comparison with the Vinnikov's approach which was considered to correct satellite data for DA effects. Since to our knowledge, Vinnikov's model has no equivalent so far, the mutual assets of both approaches for remote sensing applications are further discussed.

2. The parametric RL model

2.1. Analytical formulation

The RL model has been adapted from the reflectance model proposed by Roujean (2000) by replacing the reflectance (see expression 25 in Roujean's paper) by the surface temperature. To obey the definition of anisotropy we have adopted (i.e. difference between off-nadir and nadir temperatures), the nadir temperature (T_N) is introduced which leads to the following expression (see Eq. 1 in Lagouarde and Irvine, 2008):

$$T(\theta_s, \theta_v, \varphi) - T_N = (T_{HS} - T_N) \frac{[\exp(-kf) - \exp(-kf_N)]}{[\exp(-kf_{HS}) - \exp(-kf_N)]} \quad (1)$$

The difference $T(\theta_s, \theta_v, \varphi) - T_N$ (called ΔT) sizes the anisotropy for given zenith viewing angle (θ_v) and viewing azimuth (φ_v). The difference ($T_{HS} - T_N$) (called ΔT_{HS}) is the anisotropy in the hot spot geometry (the subscript HS stands for Hot Spot). θ_s is the solar zenith angle, and φ the relative azimuth between Sun (φ_s) and observer (φ_v). It is worth reminding that what is referred to as 'hot spot' here corresponds to the highest values of brightness temperature obtained when the viewing direction coincides with the Sun direction (Sun being

backward): this is related to the fact that in the exact Sun direction, the target displays only sunlit elements which are also the warmest ones. When the viewing direction departs from the Sun one, more and more shaded elements can be seen by the sensor and contribute to decrease the measured directional temperature. Therefore both hot spot in the thermal and in the visible/near (VNIR) infrared spectral ranges are associated to the same geometric configuration though somewhat different physical meanings may arise. In the VNIR the directional anisotropy is governed mainly by the radiative transfer processes within the canopy. In the TIR domain the coupled energy transfers are further added to the physics of DA. Indeed, these latter govern the vertical profile of the surface temperature within the canopy according to its attributes (leaf elements, stems, whorls, etc.) seen by the sensor, possibly down to the soil. This explains the dependence of TIR DA with all factors governing the energy exchanges: canopy structure (for radiation, but also wind penetration), meteorological forcing, water availability for soil evaporation and plant transpiration. In addition, thermal inertia effects could also affect the TIR directional anisotropy. At the opposite to urban canopies where a small bias of hotspot position versus Sun angles is observed (e.g., Lagouarde et al., 2010), there is no significant impact for vegetation canopies. Worth mentioning that we only treat herein the case of reference of a turbid vegetation canopy. In fact, it was already the case of the urban canopy for which Eq. (1) was originally derived. Besides, we shall examine its applicability for vegetation in what follows. The case of discrete incomplete canopies such as savannahs for instance (Pinheiro et al., 2006), sparse vegetation (Kabsch et al., 2008; Guillevic et al., 2013) or even row crops (such as vineyards, see Lagouarde et al., 2014) for which TIR directional anisotropy displays different patterns will not be investigated here.

The function f measures the angular distance between the directions of the sun beam and the observer. It is defined as:

$$f = \sqrt{\tan^2\theta_s + \tan^2\theta_v - 2 \tan\theta_s \tan\theta_v \cos\varphi} \quad (2)$$

At nadir ($\theta_v = 0$) f takes the value $f_N = \tan\theta_s$ while in hotspot geometry ($\theta_v = \theta_s$ and $\varphi = 0$) $f_{HS} = 0$. Thus Eq. 1 can be rewritten as:

$$\Delta T(\theta_s, \theta_v, \varphi) = \Delta T_{HS} \frac{[\exp(-kf) - \exp(-k \tan\theta_s)]}{[1 - \exp(-k \tan\theta_s)]} \quad (3)$$

In what follows ΔT_{HS} and k are considered to be the two parameters of the model.

Fig. 1 is provided to illustrate the potential of analytical expression (3) to describe the anisotropy, with arbitrary prescribed values $k = 0.1$ and 2 and $\Delta T_{HS} = 1$ °C and 3 °C, and with a Sun position ($\varphi_s = 210^\circ$, $\theta_s = 25^\circ$) corresponding to an acquisition time in early afternoon. The parameters k and ΔT_{HS} have here been chosen only to provide a realistic range of anisotropy values. Fig. 1a first shows the directional anisotropy (grey-color coded) simulated by RL (with $k = 2$ and $\Delta T_{HS} = 3$ °C). A polar plot representation is adopted here (see Lagouarde et al., 2010). It indicates the viewing direction (relative to the observer position): the radii are oriented according to the azimuth view angle φ_v , and concentric circles correspond to zenith view angles θ_v . A way of easily figuring this representation is to imagine a hypothetic observer placed on the vertical axis passing through the centre of the polar plot and looking at the surface in the directions corresponding to those of the polar plot. For instance, if this observer looks towards N-NE ($\varphi_v = 30^\circ$, with a zenith view angle $\theta_v = 25^\circ$), a maximum of anisotropy will be caught. This is explained by the fact the canopy elements therefore seen are those directly facing the Sun. They form the warmest elements because they only concentrate the contribution of the direct radiation beam impinging the surface. The maximum anisotropy effect obtained when viewing the surface in the exact Sun direction, with the Sun in the back, is referred to as 'hot spot'. The Sun position is also indicated in Fig. 1a by a white cross occupying a position opposite to the hot

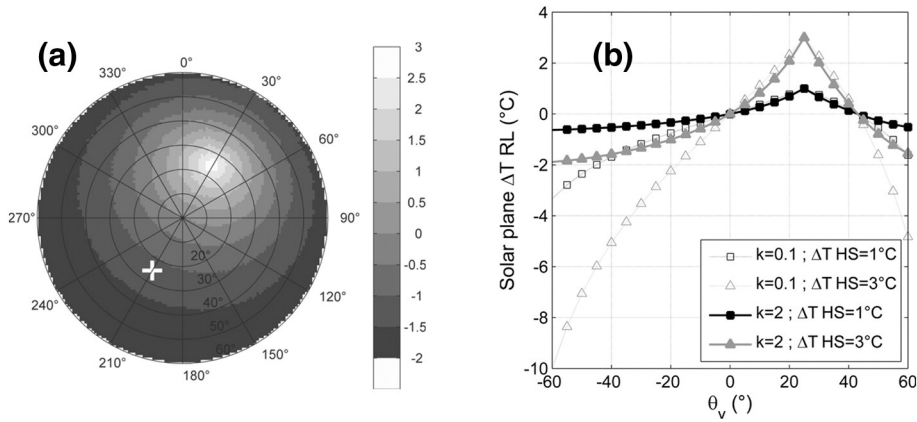


Fig. 1. (a) Polar plot of RL simulated anisotropy (grey coded) with $k = 2$ and $\Delta T_{HS} = 3^\circ\text{C}$; the radii and the concentric circles indicate the azimuth viewing angles φ_v (referred to North) and the zenith viewing angles θ_v , respectively, and the white cross corresponds the position of the Sun. (b) Anisotropy in the principal solar plane with $k = 0.1$ (empty symbols) and 2 (full symbols) and $\Delta T_{HS} = 1^\circ\text{C}$ (black) and 3°C (grey).

spot in the polar diagram. The directional structure of anisotropy rendered by Eq. (3) appears quite consistent with previous experimental results (see for instance polar plots of Fig. 2 in this paper, taken from Lagouarde et al., 2000, 2010).

Fig. 1b displays the anisotropy (i.e. $\Delta T(\theta_s, \theta_v, 0)$) computed following Eq. (3) simulated with RL in the solar principal plane for the four cases ($k = 0.1$ & $\Delta T_{HS} = 1^\circ\text{C}$; $k = 0.1$ & $\Delta T_{HS} = 3^\circ\text{C}$; $k = 2$ & $\Delta T_{HS} = 1^\circ\text{C}$; $k = 2$ & $\Delta T_{HS} = 3^\circ\text{C}$). As expected, ΔT_{HS} governs the anisotropy at hotspot while k adjusts the shape of the variations of anisotropy with the viewing zenith angles. An increase of k infers a decrease of the anisotropy amplitude over the range of variation of θ_v , with a somewhat sharper shape of anisotropy around the hotspot. This behavior was expected, as it is related to the introduction of the f function and also illustrated in Fig. 3 of Roujean (2000) paper.

The quantities k and ΔT_{HS} , both referred to as ‘parameters’ of the RL model, have not exactly the same status. According to Roujean (2000), k in the optical domain is closely related to the canopy structure, in particular leaf area index LAI, and can be approached by LAI/4 for a random foliage (i.e. spherical canopy). The possibility of using this approximation for TIR will be examined further in details in Section 3.3. The variable ΔT_{HS} quantifying the hot spot phenomenon depends on the meteorological forcing imposed at the surface and on the surface water status. Therefore ΔT_{HS} is perceived a priori as a variable rather difficult to prescribe.

In this paper, we only focus on demonstrating the ability of the RL model to properly depict the directional anisotropy. This is a necessary preamble prior to a validation exercise which will have to be performed in a second round. Indeed, this would require a calibration first of the model, meaning one should be able to set the k and ΔT_{HS} parameters to any encountered conditions. This is discussed at the end of the paper where guidelines for inversion procedure are glimpsed. Therefore the protocol we followed here simply consisted to achieve a best adjustment of the parameters of RL model in a statistical sense on the data sets, either issued from measurements or simulations. This provides an estimate of the quantities ΔT_{HS} and k resulting from the inversion procedure, to finally evaluate the error and assess the accuracy.

2.2. Experimental evaluation of RL

2.2.1. Experimental data

This section aims at demonstrating the consistency of RL model by a comparison exercise against available experimental datasets. The measurements were obtained during 2 field campaigns performed over a city (Lagouarde and Irvine, 2008) and a forest canopy (Lagouarde et al., 2000). The measurement protocol was based on the use of airborne TIR cameras embarked aboard a small aircraft. The cameras were

equipped with wide angle lenses and were mounted aboard the aircraft with an inclined angle to increase the range of zenith viewing angles investigated. Several short flight lines were flown in opposite directions all crossing at the centre of the study area (city portion or forest stand). The first line was flown in the principal solar plane and the second one within the perpendicular plane. Two additional lines were then flown in directions $\pm 45^\circ$ from the principal plane. The combination of the 8 flight segments allows one to obtain TIR directional measurements for zenith viewing angles θ_v up to 60° with a total coverage of all azimuthal viewing directions. The originality of this protocol lies in the fact it operates an averaging of both spatial non-homogeneities of the study area (streets, yards, squares, small clearings, etc.) and temporal fluctuations (due to the turbulence of atmospheric flow, see Lagouarde et al., 2015). Detailed descriptions of the protocol can be found in the 2 above-referenced papers of Lagouarde et al. (2000) and Lagouarde and Irvine (2008).

The urban area was the city centre of Toulouse and was studied in the framework of the CAPITOU experiment (Masson et al., 2008). The city centre of Toulouse spreads over an area of about 2×3 km. It is densely built with small yards or gardens inside the blocks, and only a little vegetation (about 8%) concentrated along a few streets or in parks. Most buildings are old and the materials most commonly used are brick for walls and tiles for roofs. The mean height of walls is about 15 m. Streets are oriented in all directions and display a large variety of widths. A homogeneous study area was arbitrarily delimited by interpreting airborne photos; the area was large enough to include all the characteristic elements of the city centre and to extract representative TIR anisotropy.

The second experiment was performed over a pine stand, at Le Bray ($44^\circ 43'\text{N}$, $0^\circ 46'\text{W}$), an INRA experimental site situated near Bordeaux. It was a large rectangular 350×500 m stand, 26 years old, with a 17.6 m mean height of trees (in 1996). The density was 518 trees per hectare. The mean spacing between trees was 4.7 m. The LAI was about 3.1. The ground was not fully covered by the canopy, with a crown cover estimated to be about 70%. Moreover, the stand had been planted in rows (about 35° of azimuth from North), but the spacing between rows and trees (4 and 4.7 m respectively) being nearly similar, the stand was appearing rather homogeneous.

For each surface 2 sequences of measurements acquired in the middle of the day were selected. Table 1 provides the position of the Sun at the beginning and the end of each sequence.

For every sequence of measurements (i.e. for each experimental polar plot) the fit of the RL model and retrieval of ΔT_{HS} and k was performed within the range $[0-50^\circ]$ of zenith viewing angles by step of 1° and in the range $[0-360^\circ]$ by step of 1° for azimuth directions. For this purpose, we used the automatic optimization “fminsearch” procedure,

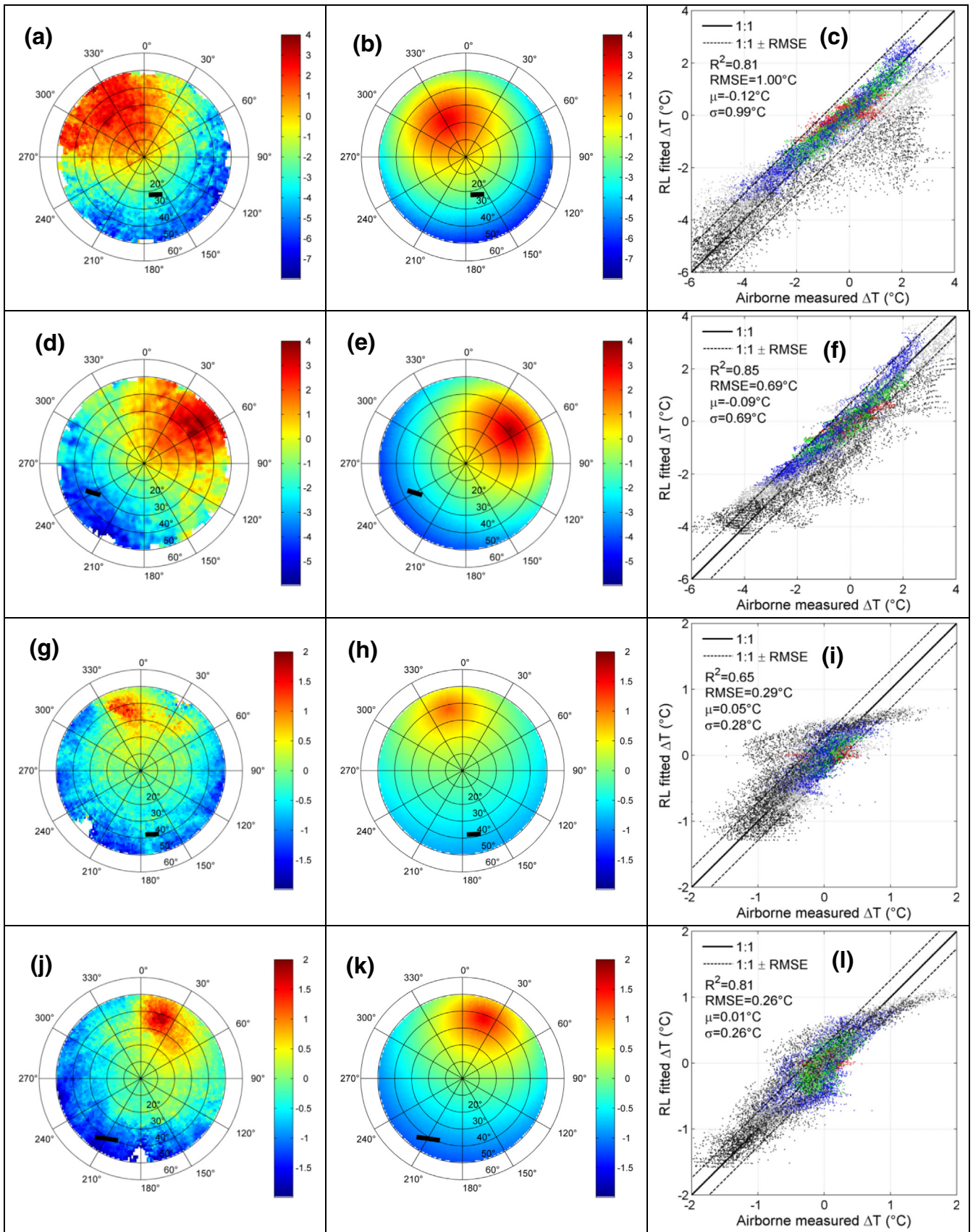


Fig. 2. Anisotropy measured above Toulouse City (July 15th, 2004) between 11:15–11:49 (a) and 13:48–14:23 UTC (d) and above a maritime pine stand at Le Bray (September 4th, 1996) between 11:20–11:52 (g) and 12:52–13:36 (j) with corresponding polar plots obtained by fitting RL model (b–e–h–k). Scatterplots of RL-simulated versus airborne measured anisotropy (c–f–i–l) are also shown, with red, green, blue, grey and black points for discriminating data in zenith intervals [0–10], [21–30], [31–40] and [41–50] respectively. (For interpretation of the references to color in this figure legend, the reader is referred to the web version of this article.)

Table 1

Characteristics of the flights performed over Toulouse and Le Bray forest sites. The duration of each flight (UTC time) is indicated. The variation of azimuthal φ_s (counted positively clockwise from North) and zenithal θ_s solar angles during observations are also provided.

Site	Date	Time (UTC)	φ_s/θ_s (begin)	φ_s/θ_s (end)
Toulouse city	2004/07/15	11:15–11:49	153.6/24.0	173.3/22.2
Toulouse city	2004/07/15	13:48–14:23	234.1/31.5	244.9/36.9
Pine forest	1996/09/04	11:20–11:52	163.1/38.7	175.8/37.6
Pine forest	1996/09/04	12:52–13:36	199.8/39.1	215.6/42.7

proposed in the MATLAB optimization toolbox. It is a multidimensional unconstrained non-linear minimization procedure, based on the Simplex algorithm (Nelder and Mead, 1965).

2.2.2. Evaluation of RL over a urban canopy

A first test of the RL model against experimental data had initially been proposed over the centre of Toulouse at 2 dates in 2004 and 2005 (October 4th, around 11:00 UTC, and February 25th, around 14:10 UTC). It is worth noting that, because of location of sites close to 0° longitude, times can be expressed indifferently in UTC or LST in this paper. The notation in UTC has been adopted in what follows. The fall and winter dates made that the hot spot was corresponding to rather large zenith solar angles, about 50 and 60° respectively, and the model had been fitted against the measured anisotropy close to the principal plane only (assembling all the measurements in the planes comprised between the principal solar plane $\pm 3^\circ$). The agreement between the measurements and RL simulations as the result of a best fit was found quite satisfactory, with correlation coefficients R^2 of 0.96 and 0.93 and root mean square errors (RMSE) of 0.5 °C and 1 °C for October 4th and February 25th respectively (see Fig. 11 of Lagouarde and Irvine, 2008, paper).

The new results presented here over the same city during the same CAPITOL experiment, but on summer conditions (July 15, 2004) have been obtained by fitting the RL model on the whole experimental dataset, i.e. for all azimuth viewing directions ($0 \leq \varphi_v \leq 359^\circ$), and for zenith viewing angles $0 \leq \theta_v \leq 50^\circ$. The results are illustrated in Fig. 2a and b for 11:30 UTC, and in Fig. 2d and e for 14:00 UTC.

The general agreement is excellent for both cases. The variation of position of the hot spot with the time of the day is also well depicted. Nevertheless a spread of high anisotropy values around the hot spot can be observed on the experimental data for azimuth viewing directions towards North, West and East. This remains unexplained for time being but it could be related to a few prevailing street directions within the city (possibly the two perpendicular 'boulevards' oriented NW-SE and NE-SW clearly visible in the aerial photography of the city (see Fig. 1 in Lagouarde et al., 2010)). The scatter plots also given (Fig. 2c and f) confirm the reliability of the RL model. It can be noticed a tendency of RL to underestimate the measurements for zenith viewing angles larger than 40°. The deviation of a group of points from the 1:1 line in Fig. 2c is clearly related to the spread of the experimental measurements around the hot spot, as mentioned just above. Despite this, the directional signatures are very well depicted with $R^2 > 0.8$ and $RMSE \leq 1$ °C.

2.2.3. Evaluation of RL over a forest canopy

Fig. 2g and j displays the polar plots of anisotropy measured during 2 flights between 11:20 and 11:52, and between 12:52 and 13:36 UTC on September 4th, 1996 (Lagouarde et al., 2000), whereas Fig. 2h and k are the corresponding RL simulations. As for urban canopies, the directional variations are correctly represented by RL. The anisotropy simulated in the immediate vicinity of the hotspot appears slightly lower than the measured one by 0.75 °C, as shown in the scatterplots provided in Fig. 2i and l. The statistics indicate $R^2 = 0.65$ and 0.81 and $RMSE = 0.29$ °C and 0.26 °C for the first and second flight respectively. The deviation between measured and fitted anisotropy above the 1:1 line noted in Fig. 2i corresponds to azimuth viewing directions φ_v around 320° for which a discontinuity appears in experimental data (Fig. 2g). The linear

structure of this discontinuity suggests a measurement artefact appearing when combining the different axes flown successively and possibly affected by different ambient micrometeorological conditions - wind speed in particular - inducing variations in surface temperature. A possible effect of row direction (35° from North) could also be invoked. However RL fits quite well the experimental data.

The preliminary consistency tests above presented over a city and a forest canopy demonstrate the potential of RL to describe DA, but the scarcity of similar anisotropy data over other surfaces and other conditions makes difficult evaluating the RL model further. Indeed a recent sensitivity study (Duffour et al., 2015a) demonstrated that TIR directional anisotropy is governed by several factors jointly: additionally to Sun position (i.e. season, date, and time of day), canopy structure (i.e. Leaf Area Index, Leaf Angle Distribution Function and hotspot parameter), meteorological forcing and surface water status. An extensive evaluation of the RL model for a large variety of situations that can be met is therefore needed. This can only be based on large simulated datasets. Next section describes this exercise using the SCOPE model as a data generator.

3. SCOPE generalization

3.1. The SCOPE model

The SCOPE model (Van der Tol et al., 2009) is a multi-layer SVAT model developed for the combined simulation of directional reflected solar radiation, emitted thermal radiation and sun-induced fluorescence signals at TOC (Top of Canopy) of homogeneous canopies together with energy, water and CO₂ fluxes. It is based on a combination of several models describing radiative, turbulent and mass transfers inside the canopy, taking into account leaf biochemistry and aerodynamic processes. Associated to the multilayer approach, this latter vision was deemed well appropriate to treat the case of turbid canopies. This explains our final choice for SCOPE among other existing models such as for instance CUPID/TGRM (Huang et al., 2008) or even DART (Gastellu-Etchegorry et al., 2004). The main features of the model are briefly recalled here. For more details, the reader is referred to the paper introducing the SCOPE model.

In SCOPE model, the canopy is described through the prescription of 60 horizontal layers for vegetation, and 1 layer for soil. Classical parameters are used to account for the canopy structure in vegetation layers, such as LAI, leaf angles distribution or gap fractions probabilities. Leaves are distributed in 13 zenithal per 36 azimuthal directions. The unified 4SAIL model (Verhoef et al., 2007) is used to simulate the radiative transfer. It computes net radiation and radiances within the [0.4–50] μm spectral range. In the optical range ([0.4–2.5] μm) the PROSPECT model (Jacquemoud and Baret, 1990) is used to derive reflectance and transmittance spectra for vegetation. For wavelengths beyond 2.5 μm, leaves emissivity is prescribed to 0.97 and transmittance is assumed to be 0. For the soil, a reflectance spectrum must be provided.

The computation of energy fluxes (sensible heat, latent heat, soil heat) and CO₂ fluxes is based on biochemical and aerodynamic processes. Biochemical processes involve the Cowan's model (Cowan, 1977) to compute stomatal conductance. The Farquhar et al. (1980) leaf photosynthesis model is using the carboxylation capacity ($V_{c_{\text{mo}}}$) as input, a parameter controlling the photosynthetic capacity. Aerodynamic resistances are computed from the Wallace and Verhoef (2000) approach and the soil surface resistance (r_{ss}) can be prescribed or slaved to soil moisture.

Additionally to fluxes, SCOPE enables computing directional reflectances in the solar domain and directional brightness temperatures in the thermal domain (between 8 μm and 14 μm). The directionality results both from the combination of the probability of viewing - or not - a leaf or a soil element, and of the probability of being sunlit/shaded for soil or leaves. These probabilities are computed for each vegetation layer, which enables estimating the radiances emitted by shaded and sunlit

leaves and soil seen by the observer in a given direction above the canopy. By summing these radiances (for more details see Eq. 28–35 in Van der Tol et al., 2009) we obtain the directional radiance at top of canopy (TOC), $L(\theta, \varphi)$, which is transformed into a directional brightness temperature $T_b(\theta, \varphi)$ according to the Stefan-Boltzmann equation:

$$\pi L(\theta, \varphi) = \sigma T_b^4(\theta, \varphi) \quad (4)$$

where σ is the Stefan Boltzmann constant ($5.67 \cdot 10^{-8} \text{ W} \cdot \text{m}^{-2} \text{ K}^{-4}$).

The ability of SCOPE to simulate the energy fluxes as well as TIR directional brightness temperatures and directional anisotropy at TOC was evaluated by Duffour et al. (2015b). These authors first compared the results of simulations to two ground experimental datasets measured on winter wheat and a maritime pine stand for which latent and sensible heat fluxes with CO_2 assimilation were available. Complementary to these data directional brightness temperatures were measured towards North and South on the winter wheat site. On the maritime pine stand, a set of measurements of the directional brightness temperature was made towards West, and a second set was made with measurements made at hotspot, the radiothermometer being mounted on a motorized platform slaved to Sun position all along the day. A mean RMSE of about 30 and $50 \text{ W} \cdot \text{m}^{-2}$ was found for latent and sensible heat fluxes respectively, while for directional brightness temperatures, the RMSE ranged between 1 and 1.5°C . A second part of the study demonstrated that the SCOPE model could qualitatively simulate directional signatures of anisotropy (the difference between off-nadir and nadir temperatures) successfully. This

comparison - which was in no way a validation of SCOPE - was done against the forest canopy dataset used in Section 2.2.3. Rather, the SCOPE-simulated dataset and the experimental dataset over the forest canopy yielded independent source of information for fitting the parametric models studied in the paper (RL and further Vinnikov's).

3.2. Generation of a synthetic dataset

Using SCOPE as a data generator we created a synthetic dataset of TIR directional anisotropy. This is the dataset which has been used by Duffour et al. (2015a) to study the sensitivity of directional anisotropy to its governing factors. The input values prescribed to these factors are recalled here for the sake of convenience. We consider they allow to generate a representative range of anisotropy effects to be met in practice. SCOPE simulations were made at 13:00 UTC for two days under cloud free conditions close to spring equinox (DoY 79) and to summer solstice (DoY 174). These dates were chosen to have a large change both in forcing global radiation and solar position. We also run simulations on DoY 354 (close to winter solstice) but anisotropy revealed to be very low at this season (no $>0.5^\circ\text{C}$) on the range of zenith viewing angles considered in this study ($\theta_v < 50^\circ$), due to a low global radiation and a position of hot spot located at large zenith angle ($>65^\circ$); the results obtained on this day were considered as non-significant and therefore discarded here. We focused on the 13:00 time because it corresponds to the overpass time of a future TIR spatial mission (Lagouarde et al., 2013). However, limiting the dataset to a single time do not jeopardize its degree of representativeness because the

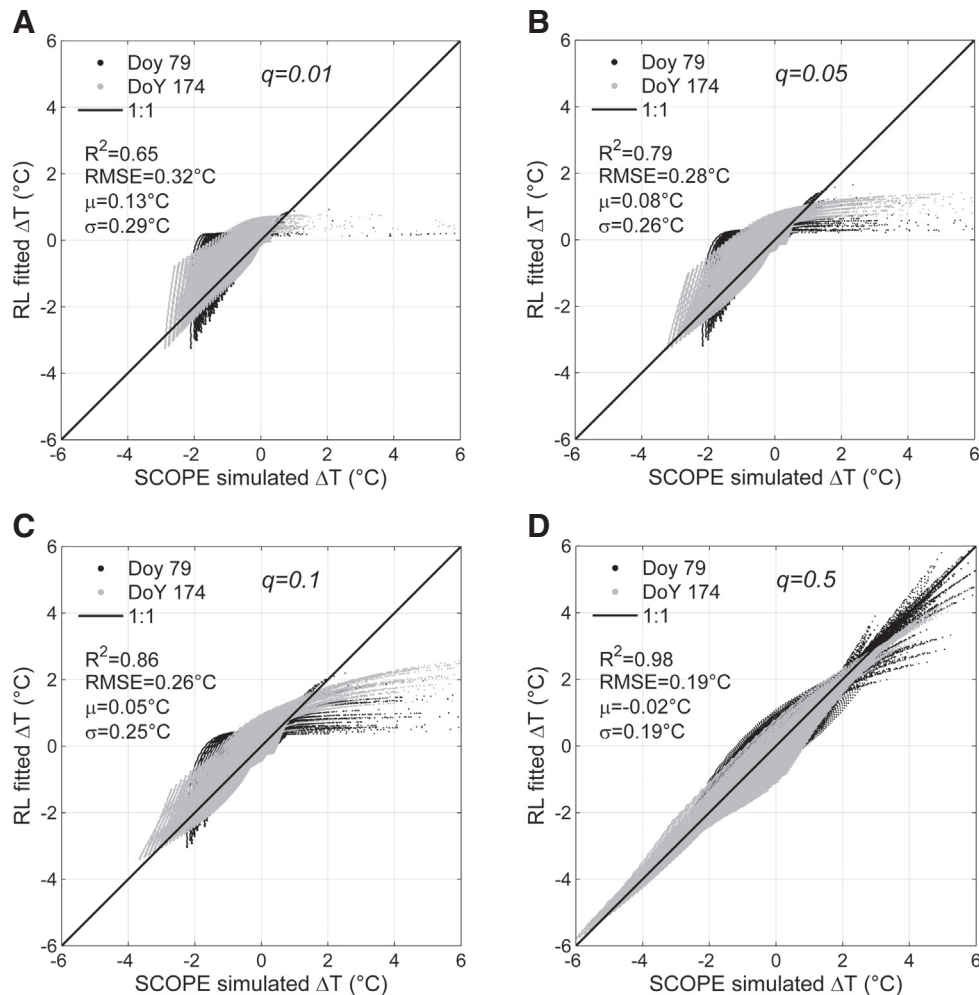


Fig. 3. Comparison of RL-fitted against SCOPE-simulated anisotropy for DoY 79 and 174, and for $q = 0.01$ (a), $q = 0.05$ (b), $q = 0.1$ (c) and $q = 0.5$ (d).

variability of forcing conditions throughout the day is likely to be partly reproduced through the variability between dates.

The main input meteorological data (global radiation, longwave downward radiation, and air temperature and humidity) were taken from the Auradé station, located near Toulouse (France) (Béziat et al., 2009, http://www.cesbio.ups-tlse.fr/data_meteo/index.php?perma=1378392362), which constrains our study at $\sim 45^\circ$ latitude. The wind speed was set at a constant value of $2 \text{ m}\cdot\text{s}^{-1}$ since Duffour et al. (2015a) found that its impact on anisotropy was low, contrary to other conditions such as surface water status or global radiation. We simulated a 1 m height canopy with a spherical leaf angle distribution function. Different canopy structures were created by prescribing 6 Leaf Area Index ($\text{LAI} = \{0.5, 1, 1.5, 2, 3, 5\}$) and 4 values of the hot spot parameter q defined as the ratio between leaves size and height of the canopy (0.01, 0.05, 0.1 and 0.5). 4 water statuses are considered by crossing wetness/dryness of soil/vegetation (all humid, all dry, humid soil/dry vegetation, dry soil/humid vegetation) as follows. For vegetation, the maximum of carboxylation, V_{cmo} (a parameter related to the photosynthetic activity and therefore to the stomatal conductance), is prescribed at 125 and $25 \mu\text{mol}\cdot\text{m}^{-2}\cdot\text{s}^{-1}$ to simulate high and low stomatal conductance respectively, i.e. to simulate well-watered and dry conditions. For the soil, the surface resistance (r_{ss}) is set at 200 and $2000 \text{ s}\cdot\text{m}^{-1}$, which corresponds to wet and dry conditions respectively. The marginal cost of assimilation, a parameter governing the stomatal conductance, is set at $2000 \text{ mol}\cdot\text{mol}^{-1}$. The resulting simulated dataset is composed of about 200 cases. For each of them the anisotropy is computed for all directions from 1° to 360° and from nadir to 50° zenith by steps of 1° . The limitation in zenith is justified since it corresponds to the useful range of zenith view angles for current large swath instruments such as MODIS or VIIRS. Indeed despite that maximum scan angles of $\sim 55^\circ$ result in $\sim 65^\circ$ zenith view angle at swath edge for these sensors, we consider that beyond 50° zenith view angles, measurements are often too much contaminated by atmospheric effects.

3.3. Comparison of RL and SCOPE directional anisotropy

Fig. 3a–d shows the anisotropy obtained with the RL model adjusted on SCOPE simulated data for the complete dataset. The results are presented discriminating the hot spot parameter values, from $q = 0.01$ (Fig. 3a) to $q = 0.5$ (Fig. 3d) respectively.

The strong impact of q parameter is conspicuous. It first appears that there is a global agreement between the RL and SCOPE simulated values, and that the range of anisotropy values increases with q . Nevertheless for q values up to 0.1 (Fig. 3a–c), and particularly for $q = 0.05$ and $q = 0.01$, we can observe a deviation from the 1:1 line, which corresponds to SCOPE anisotropy values larger than 2°C . It has been checked that these correspond to points situated in the vicinity of the hot spot. This can be explained by a rather sharp shape of the hot spot which cannot be described with Eq. 1. Despite the representation may be misleading, the density of points within the greyish and black areas deviating from the 1:1 line in Fig. 3b and c, is in fact not so important. For $q = 0.5$, the agreement between RL and SCOPE is excellent. The computation of the RMSE and the R^2 confirms the global quality of the fit of RL against SCOPE: R^2 increases with q from 0.65 for $q = 0.01$ to 0.98 for $q = 0.5$, while RMSE decreases from 0.32°C for $q = 0.01$ to 0.19°C for $q = 0.5$. RMSE is equal to 0.28°C and 0.26°C for $q = 0.05$ (Fig. 3b) and $q = 0.1$ (Fig. 3c) respectively. However, although a large range of values can be found in literature for the q parameter in the context of the simulation of directional reflectance in the solar domain, there are no indications about the possibility of prescribing them directly to the TIR domain.

Another illustration of the ability of RL model to describe the anisotropy satisfactorily, and simultaneously a confirmation of the limited weight of discrepancies in the hot spot region is given in Fig. 4 which shows the histogram on the deviations between RL and SCOPE data

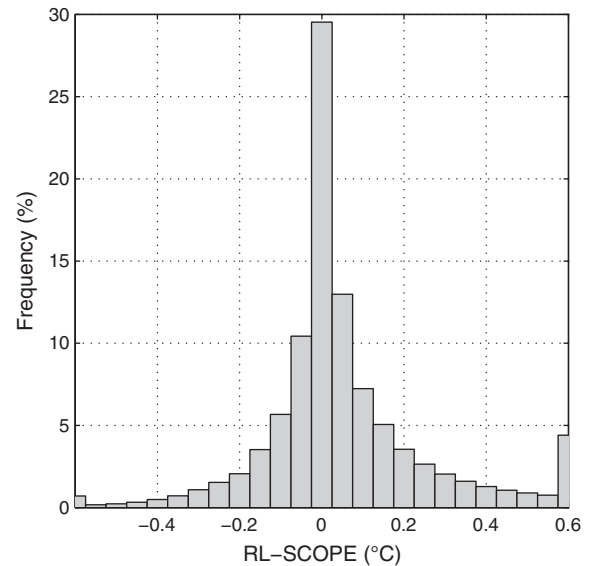


Fig. 4. Histogram of the difference between RL-fitted and SCOPE-simulated anisotropy.

(full dataset included). It is centred on 0°C and shows a slight asymmetry. The very small peak appearing on the left side corresponds to hot spot data and indicates that $<1\%$ of the differences between RL and SCOPE are lower than -0.6°C . The other peak on the right side of the histogram corresponds to data for which RL overestimates SCOPE anisotropy by $>0.6^\circ\text{C}$. A detailed analysis of the result of the fit of RL against SCOPE has shown that these large differences mainly take place in the case of dry soils with LAI ranging between 1 and 2. The cumulated histogram of the distribution of the absolute difference between RL and SCOPE data (not presented here) reveals that the discrepancies between the two models fall within 60% and 90% for values lower than 0.1°C and 0.4°C , respectively. Finally, only 5% of the data differ of $>0.6^\circ\text{C}$.

Owing to an optimum retrieval of the two parameters of the RL model, TIR directional anisotropy is nicely reproduced compared to SCOPE data. A thorough analysis of the retrieved parameters ΔT_{HS} and k shows that such information cannot be set to a priori values since they don't follow obvious trends as a function of the main drivers of anisotropy, i.e. global radiation, canopy structure and water status. As mentioned previously, Roujean (2000) demonstrated that in its expression derived to simulate optical hotspot BRDF, the parameter k could be set to $\text{LAI}/4$ for spherical canopies. In the present exercise the retrieved k values were varying with LAI and q without making possible to find a simple parameterization of k . Moreover k took negative values for some cases with $q = 0.01$ on DoY 174 and with q up to 0.1 on DoY 79. In the present status of our study we therefore could not prescribe k to $\text{LAI}/4$, which made necessary fitting both k and ΔT_{HS} in the inversion of the RL model. Nevertheless we suggest further research to be done here. Indeed the attempts of inversion we made with $k = \text{LAI}/4$ were not accurate enough, but several reasons could be argued: is it because the input parameters have been crossed in SCOPE without any constraints, so generating unrealistic situations? Is it because of a lack of realism in the SCOPE simulated hot spot, which is difficult to assess because not documented in literature to our knowledge?

We have shown that RL performs well in a case study with meteorological data (in particular Sun zenith angles) which can be met close to 45° latitude. One can wonder if it could be used in the inter-tropical zone where the sun is at zenith ($\theta_s = 0^\circ$) twice a year. Indeed in such geometrical configuration, ΔT_{HS} tends to 0°C since the hotspot position and the nadir coincide. This result must be studied more in details with real datasets measured at these latitudes but, in the framework of this study, we cannot conclude on the possibility to prescribe k to $\text{LAI}/4$.

4. Comparison between RL and Vinnikov capabilities

4.1. The Vinnikov kernel approach

Vinnikov et al. (2012) developed a parametric model based on three kernels designed to normalize LST measured by satellites:

$$\frac{T(\theta_s, \theta_v, \varphi)}{T_{nadir}} = 1 + A \cdot E(\theta_v) + D \cdot S(\theta_v, \theta_s, \varphi) \quad (5)$$

with $T(\theta_v, \theta_s, \varphi)$ the temperature (in Kelvins) measured off-nadir and T_{nadir} the temperature at nadir (in Kelvins). The first term '1' plays the role of the 'isotropic' kernel, i.e. it enables setting the ratio $\frac{T(\theta_s, \theta_v, \varphi)}{T_{nadir}}$ to 1 when $T(\theta_s, \theta_v, \varphi)$ is measured at nadir.

$E(\theta_v)$ and $S(\theta_v, \theta_s, \varphi)$ are described as an 'emissivity' kernel and as a 'solar' kernel respectively. They are given by:

$$E(\theta_v) = 1 - \cos(\theta_v) \quad (6)$$

$$S(\theta_v, \theta_s, \varphi) = \sin(\theta_v) \cos(\theta_s) \sin(\theta_s) \cos(\theta_s - \theta_v) \cos(\varphi) \quad (7)$$

A and D are the corresponding coefficients of the emissivity and solar kernels. Vinnikov et al. (2012) propose a universal value for A ($A = -0.0138 \text{ K}^{-1}$) which results in a one parameter model, D becoming the only parameter to adjust.

Currently this model is the only one which might correct satellite data from directional effects. RL could also appear as a candidate for this purpose. This is why the two approaches are now compared.

4.2. Comparison between RL and Vinnikov capabilities

This comparison aims at evaluating the differences between the two models and at studying the possible efficiency of RL to correct satellite LST measurements. The synthetic dataset generated with SCOPE and introduced in Section 3.2 is taken as the reference.

Vinnikov et al. (2012) suggest the A parameter of their model to have a universal value, which makes this approach a 1-parameter approach contrary to RL which requires two parameters k and ΔT to be known. However, the Vinnikov model can also be used as a two parameters approach as done in Pires et al. (2015). Three results of modeled anisotropy are therefore compared:

- RL adjusted by retrieving both k and ΔT
- Vinnikov adjusted by retrieving only D (with $A = -0.0138 \text{ K}^{-1}$)
- Vinnikov adjusted by retrieving A and D .

The two approaches don't use exactly the same definition of anisotropy: Vinnikov et al. (2012) define it as the ratio between off-nadir to nadir temperature while RL considers anisotropy as the difference

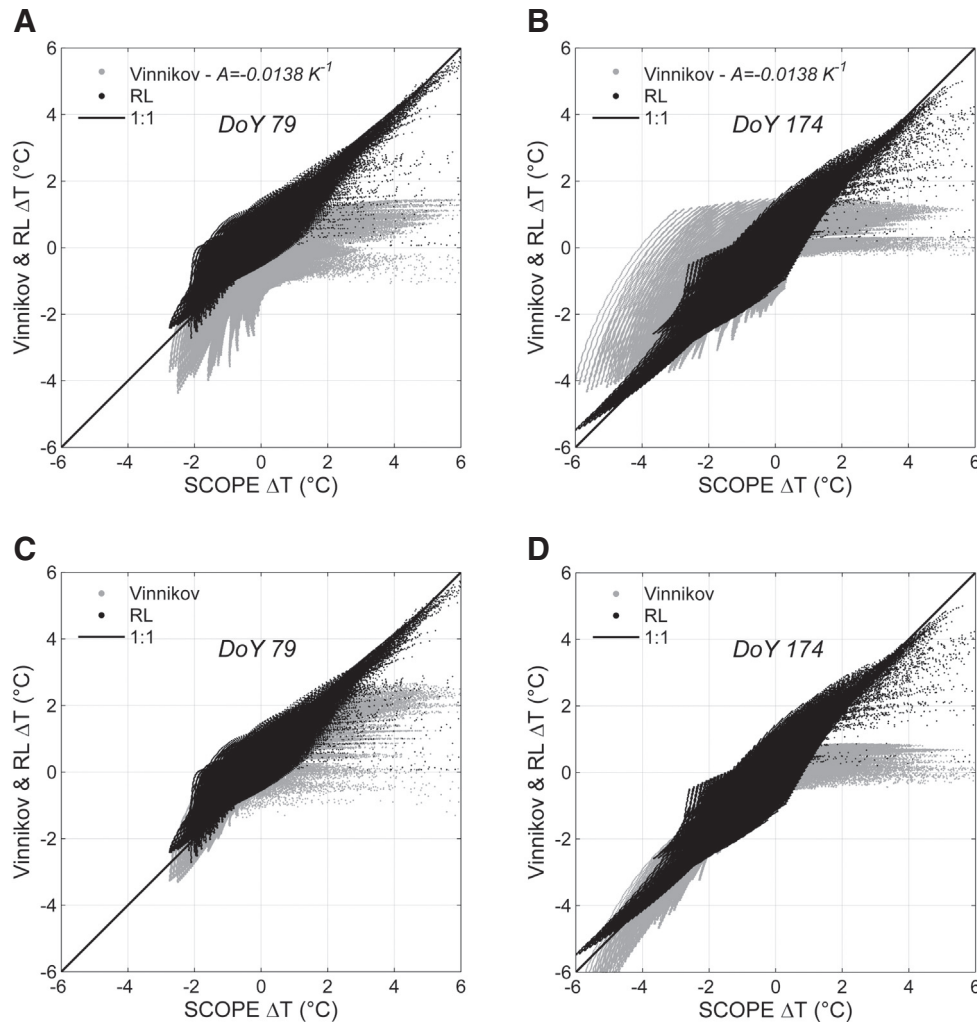


Fig. 5. Comparison of RL-fitted (black) and Vinnikov-fitted (grey) anisotropy against SCOPE-simulated anisotropy for DoY 79 (a, c) and 174 (b, d). In (a) and (b) Vinnikov's model is adjusted on D only ($A = -0.0138 \text{ K}^{-1}$) while in (c) and (d) it is adjusted on A and D .

between these. For an easier interpretation of the results we preferred to use this second definition. Vinnikov's Eq. 5 turns therefore to be:

$$T(\theta_s, \theta_v, \varphi) - T_{nadir} = T_{nadir} (A \cdot E(\theta_v) + D \cdot S(\theta_v, \theta_s, \varphi)) \quad (8)$$

Fig. 5 displays the anisotropy as simulated by the two models as a function of anisotropy simulated by SCOPE. The results obtained with Vinnikov's model adjusted on D only for DoY 79 and 174 are given in Fig. 5a and b respectively. The two corresponding lower figures (Fig. 5c and d) are for Vinnikov adjusted with two parameters. Whatever the DoY, the model of Vinnikov displays much more dispersion than the RL model when A is prescribed to -0.0138 K^{-1} . Statistics confirm that RL performs better than Vinnikov with RMSE between SCOPE and RL of $0.26 \text{ }^\circ\text{C}$ for the two days, while it reaches about $0.55 \text{ }^\circ\text{C}$ between SCOPE and Vinnikov. Similarly, the correlation coefficients R^2 between SCOPE and RL are 0.84 and 0.92 for DoY 79 and 174 respectively ($R^2 = 0.9$ for the whole dataset) against 0.59 and 0.65 between SCOPE and Vinnikov. The comparison of Fig. 5a–b on the one hand against Fig. 5c–d on the other hand clearly shows that prescribing A seems to be too much constraining in the general case. The fact it appeared satisfactory in the Vinnikov's paper could possibly be explained by the particular case study of geostationary satellite data for which the large pixel scale induces a smoothing effect and less dispersion in the resulting directional variability. This smoothing effect results from two different sources. First the spatial variability of the land use - patch of fields for instance - generally occurs at a much lower scale than the pixel size. Geostationary satellite pixels contain mixed information that appear rather similar. It is likely to reduce possible impact of mis-registration errors when associating pixels from two different satellites at different view angles. Second, as recently shown by Lagouarde et al. (2015), the limitation of surface temperature temporal fluctuations (i.e. uncertainty) induced by atmospheric flow turbulence over large pixels could also be invoked. Fig. 5c and d shows that the performances of the Vinnikov's model are significantly improved when fitted using the two A and D parameters and RMSE become $0.23 \text{ }^\circ\text{C}$ and $0.35 \text{ }^\circ\text{C}$ for DoY 79 and 174 respectively (RMSE = $0.3 \text{ }^\circ\text{C}$ when the whole dataset is compared) and $R^2 = 0.86$ for each day. For DoY 79, statistics of Vinnikov's approach are even slightly better than for RL. Nevertheless the results remain better with the RL model. In particular, despite difficulties in both cases, the simulation of the anisotropy in the vicinity of

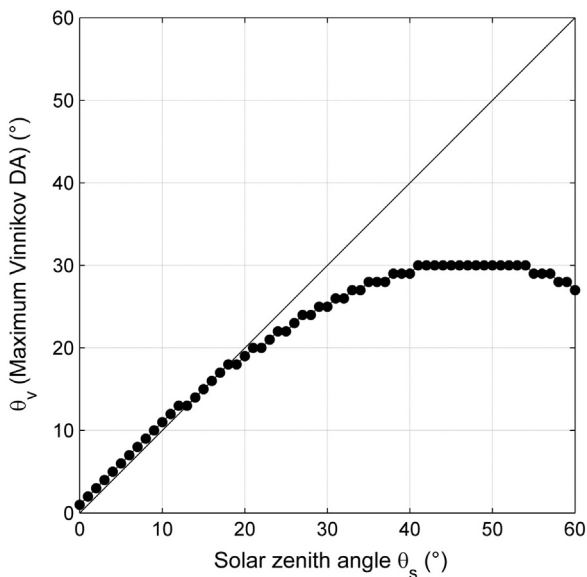


Fig. 6. Comparison of the zenith viewing angle for which the Vinnikov's model reaches its maximum of anisotropy against solar zenith angle (computations made with values $A = -0.0138 \text{ K}^{-1}$ and $D = 0.0140 \text{ K}^{-1}$ given in Vinnikov's paper).

the hot spot (which corresponds to the points deviating under the 1:1 line) is of poor quality with the Vinnikov's model. Indeed, Eq. 5 fails to depict the hot spot correctly. Fig. 6 helps to understand this issue: it shows that the zenith angle for which the maximum of anisotropy is simulated (with values $A = -0.0138 \text{ K}^{-1}$ and $D = 0.0140 \text{ K}^{-1}$ from Vinnikov's paper) doesn't correspond to the solar zenith angle, whereas it should according to the definition of the hot spot.

Finally, it seems that the two models should rather be used as two parameters approaches. Indeed, with the prescription $A = -0.0138 \text{ K}^{-1}$, the performances of the Vinnikov model are not satisfactory and lower than the RL model. We also note that Pires et al. (2015) don't follow this prescription and they propose to use the Vinnikov model as a two parameters approach, with A and D to adjust.

5. Discussion

5.1. Limitations of the parametric approaches

The issue which prevents the Vinnikov approach from being efficient to correct anisotropy close to the hotspot is partly due to the use of unadapted kernels. The RL model has been developed on the assumption that optical and TIR anisotropy behave identically, and it has been derived from a model developed for the solar domain which is based on physical considerations, not wavelengths dependent, and fully justified in Roujean (2000). Especially the introduction of the 'distance' between the Sun and view directions (Eq. 2) seems to be essential for the quality of such a simplified method. This is confirmed by Jupp (2000), who discusses the interest of introducing the phase angle in kernels development. The lack of such an angle in Eq. 5 is likely to severely weaken the Vinnikov's model.

Nevertheless, a mathematical under determination appears in RL formulation when the Sun is at nadir ($\theta_s = 0^\circ$) because the denominator in Eq. (1) tends to 0, which makes the computation of anisotropy impossible. This particular geometry occurs only twice a year only in the inter-tropical zone. In this case, the nadir viewing and hotspot position coincide, leading to $\Delta T_{HS} = 0$, with negative values of anisotropy for other viewing geometries. A study still remains to be performed in order to evaluate how to cope with this caveat for practical applications. Nevertheless, preliminary tests have been made fitting the RL model on a directional anisotropy dataset generated with SCOPE over Congo (4.5° S , 12° E) using an input meteorological dataset available at the laboratory, with a date and time chosen (DoY 28, October 8, 11:00) for having a solar zenith angle close to 1° . The results revealed very promising with an excellent fit of RL on SCOPE simulations still being possible, but further work is required for confirmation.

A common caveat of RL and Vinnikov's approaches is their non-reciprocity. The reciprocity is a mathematical property which expresses that a multi-variables function remains invariant by inverting two of its variables. In our case the reciprocity should be verified by inverting solar and viewing zenith angles: the shadows created by the Sun would become hidden elements for an observer, and conversely. Kernel models developed in the solar domain always verify this condition, and we might suppose that it is true in TIR. However, neither Vinnikov nor RL verifies the reciprocity. The first because of its empirical development, and the second, contrary to the model initially developed by Roujean (2000), because of the definition of anisotropy which is referred to nadir.

Finally, as both RL and Vinnikov's model have been tested against SCOPE-simulated anisotropy data, the question rises if the confidence in the results of this exercise cannot be biased by the quality of SCOPE. In particular the prescription of the hotspot parameter in SCOPE might be questionable. The definition of the thermal hot spot shape is little documented in literature and requires further research and experimental characterization.

Despite the aforementioned limitations we can notice that both RL and Vinnikov's approaches implicitly take into account the main drivers

of anisotropy (Duffour et al., 2015a), on one hand the meteorological forcing (which governs ΔT_{HS} and T_{nadir}) and on the other hand the canopy structure (through the k parameter and the 'emissivity' kernel).

5.2. Applications of RL to field and satellite data

5.2.1. Qualitative assessment of field measurements

Additionally to remote sensing, several applications can be found to the RL model. It may serve to assess the directional variability of thermal anisotropy but also can be of great support for designing ground experimental protocols. In this respect, it may help determining the optimum setting of TIR radiometers or cameras according to FOV, inclination angle of instruments, location and time of year for instance, and to anticipate the meaning and the quality of measurements.

5.2.2. Qualitative assessment of anisotropy on satellite data

The RL model can help to define some specifications for future LEO missions in the thermal infrared, in particular the combined choice of overpass time and orbit inclination. Fig. 7 shows the possible positions of the hot spot throughout the day, between 8:00 and 16:30 UTC, and throughout the year, between winter and summer solstices, at three latitudes, Equator, Northern Tropic and 45° North (the longitude is 0°). The positions of the hot spot at specific local time 10:30 (approximately Landsat and MODIS/TERRA overpass), 13:30 (NOAA/AVHRR, MODIS/AQUA, SUOMI NPP and planned future missions overpass) and 16:00 have been indicated by different symbols. Also indicated by arrows are the directions of scan lines for a polar orbiting mission for two orbit inclinations. In order to reduce the impact of directional anisotropy effects on measurements, it seems preferable the scan line to be as close as possible to the perpendicular solar plane: it both minimizes the amplitude of anisotropy and makes it symmetrical on each side of the satellite ground track. Therefore, from Fig. 7 it can be seen that an orbital inclination according to a flight azimuth >0 (resp. <0) is recommended for an overpass in the beginning of the afternoon at 13:30 (resp. in the mid-morning at 10:30). At the North Tropics (Fig. 2b), the same holds for winter months. But for summer months, the measurements are prone to hot spot effects whatever the orbit inclination is. Similarly, close to the Equator the previous recommendation still holds, but for spring and fall monthly periods. In the Southern hemisphere (not shown), the position of the hot spot is shifted in the opposite direction so that the same analysis can be made and that the same recommendation will remain still valid.

The RL model could reveal particularly usefulness to achieve a first qualitative assessment of directional effects for the ECOSTRESS ([\[ecostress.jpl.nasa.gov/\]\(http://ecostress.jpl.nasa.gov/\)\) mission consisting of installing the Prototype HypsIRI Thermal Infrared Radiometer \(PHYTIR\) instrument aboard the International Space Station \(ISS\). Indeed its low inclination orbit \(\$\sim 51.6^\circ\$ \) and the fact it is not Sun-synchronous make that a very large range of viewing geometries is obtained, having azimuth view angles in all directions and zenith view angles corresponding to the maximum scan angle up to \$25.5^\circ\$.](http://</p>
</div>
<div data-bbox=)

5.2.3. Correction of TIR directional anisotropy on space data

The inversion problem is a major concern before the RL model can be practically applied for correcting satellite data from DA effects. In the VNIR domain, reasonable made assumption is that vegetation canopies will not show too rapid changes over periods of a few days, typically the week. Therefore, the accumulation of satellite measurements in this range period under different viewing angles will support the inversion of kernel-based models to perform analysis and correction of anisotropy effects. This is not possible in the thermal infrared because the surface temperature is continuously varying with forcing conditions (meteorological variables) and water status (rainfall, irrigation). Vinnikov's approach proposed to solve this issue by combining 3 measurements from geostationary satellites GOES E and GOES W over US, both at nighttime and daytime, to determine the 2 kernel coefficients and the nadir temperature. Such an approach would be however impossible for other locations, such as Europe or Africa, for which no overlap between geostationary satellites can be found. The problem remains entire with LEO satellites for which only a single measurement per day over a given pixel can be obtained.

To cope with the problem of directional anisotropy, in recent projects such as MISTIGRI (Lagouarde et al., 2013) or THIRSTY (Crebassol et al., 2014), it has been proposed to fix the orbit ground track, so that every point at the Earth surface is always observed under the same viewing angles. Despite the variations of Sun angles throughout the year cannot be ignored, this specification (constraint) has been set for ease of analysis of temporal series of surface temperature at a given location. To correct for TIR DA with such an orbit, it could be suggested to take advantage of spatial variability instead of temporal variability as for VNIR domain, performing the inversion on a few pixels with the same vegetation canopy selected along the scan line. Nevertheless this obviously requires some necessary assumptions about similar water status and forcing conditions in particular, and to correct for differences in local time. Despite these assumptions appear rather constraining, it should be worth to be tested with the available land use information derived from VNIR channels.

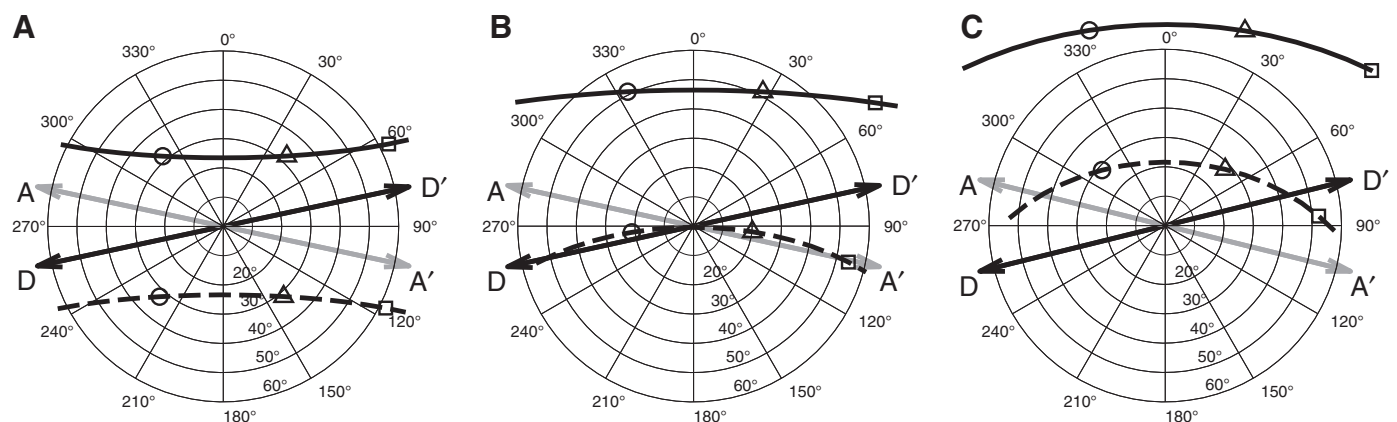


Fig. 7. Hotspot position from 8:00 to 16:30 UTC for a pixel located at latitudes 0° (a), 23° North (b) and 45° North (c) for summer (dashed lines) and winter (solid lines) solstices. Circles, triangles and squares indicate the hotspot position at 10:30, 13:30 and 16:00 UTC. AA' and DD' are the scan planes of ascending and descending orbits respectively possibly met for a polar sun-synchronous satellite.

6. Conclusion

The need for correcting satellite LST measurements from the directional effects incites to develop simple methods which could be implemented into satellite data processing chains. The simple directional anisotropy model proposed in this paper (and referred to as 'RL') is adapted to continuous turbid canopies; it requires two parameters (ΔT_{HS} representing the anisotropy at hotspot and k more related to the canopy structure) to be known. We first demonstrated its ability to reproduce TIR directional signatures by fitting it against experimental datasets over a urban canopy (Toulouse City) and over a forest canopy (maritime pine stand). Results were very encouraging with a satisfactory simulation of the hot spot and RMSE values estimated over a large range of viewing directions (all azimuth directions, zenith viewing angles up to 50°) lower than 1°C . Then, in a purpose of generalization, the RL model was tested against SCOPE simulated data crossing different input conditions of meteorological forcing, structure of the canopy and water status of soil and vegetation, to simulate most of the situations which can practically be met. On the range $[0-50^\circ]$ for θ_v and $[0-360^\circ]$ for φ_v , the agreement was rather good with a $\text{RMSE} \leq 0.6^\circ\text{C}$. Some discrepancies were observed in the vicinity of hot spot, the RL model being unable to simulate very sharp hot spot shapes accurately. However, the modeling of the hot spot and the extreme sensitivity of SCOPE to the hot spot parameter q still pose problem. A better knowledge of hot spot is therefore essential to assess the performance of RL. We also pointed out the fact that when the hotspot and the nadir coincide, i.e. when the Sun is at zenith ($\theta_s = 0^\circ$), the RL model is undetermined. A study must be carried out to evaluate the behavior of the model in this particular configuration which occurs twice a year in the whole inter-tropical zone.

Simple parametric approaches to correct satellite LST measurements are still rare and the method proposed by Vinnikov et al. (2012) is currently the only one available to our knowledge. This method was compared to the RL model using the same SCOPE simulated anisotropy dataset. The RL model reveals more efficient than Vinnikov's one to simulate DA, in particular close to the hot spot where the latter fails, probably because of unadapted kernels. Nevertheless despite some constraints - study areas seen by 2 satellites simultaneously and far enough from hot spot - the Vinnikov's approach has the advantage of easy inversion and realistic results, and it has already been implemented for practical correction of geostationary satellite data.

The RL model appears to be conceptually as a relevant model because it provides a much better description of DA close to hot spot. It has been shown that, in its present state, it can help to assess qualitative assessments of DA for various purposes: preparation of field experiments, critical analysis of measurements found in literature, help to the definition of spatial missions. However, significant research work remains to be done to transform RL model in a practical tool for correcting DA on satellite data. Several directions currently explored at the laboratory are just briefly evoked here. First, ancillary data could be introduced to improve the RL model. The air temperature is a candidate as the water status is indirectly related to actual evaporation itself linked to the difference between surface and air temperature. Similarly VNIR anisotropy derived from VNIR measurements could provide an information linked to the canopy structure. Second, efforts are carried on to improve the understanding of the hot spot phenomenon, and field experiments using UAVs (Unmanned Aerial Vehicles) are undertaken for this purpose. Finally, strategies to develop inversion methodologies of RL to correct DA for LEO satellites are studied to cope with the impossibility of acquiring imagery simultaneously in different viewing conditions. A possible approach could therefore be performing model inversion over fields with identical crops seen under different viewing angles, after verification of their close surface temperature. These studies should open up the way to the implementation of the RL algorithm in the processing of data from satellites such as MODIS, SUOMI NPP, or future high spatial resolution/high revisit TIR missions in preparation phase.

Acknowledgments

This work was supported by the 'Centre National d'Etudes Spatiales' (CNES) and the 'Institut National de la Recherche Agronomique' (INRA) Department of 'Environnement et Agronomie' who co-funded Clément Duffour's PhD. We thank Region Aquitaine, ANR 'Investissement d'Avenir' (Equipex XYLOFOREST) who funded and provided facilities and data used in this thesis and also in the paper by Duffour et al. (2015b) (Remote Sens. Environ., 158, 362–375). We are also grateful to the TOSCA ('Terre, Océan, Surfaces Continentales, Atmosphère') CNES group for his support and to the CESBIO and CIRAD who provided meteorological data.

References

- Béziat, P., Ceschia, E., Dedieu, G., 2009. Carbon balance of a three crop succession over two cropland sites in South West France. *Agric. For. Meteorol.* 149, 1628–1645. <http://dx.doi.org/10.1016/j.agrformet.2009.05.004>.
- Bréon, F.-M., Maignan, F., Leroy, M., Grant, I., 2002. Analysis of hot spot directional signatures measured from space. *J. Geophys. Res.* 107, 4282. <http://dx.doi.org/10.1029/2001JD001094>.
- Cowan, I., 1977. Stomatal behaviour and environment. *Adv. Bot. Res.* 4, 117–228.
- Crebassol, P., Lgouarde, J.-P., Hook, S., 2014. Thirsty thermal infrared spatial system, 2014 IEEE Geoscience and Remote Sensing Symposium. Quebec City, QC 3021–3024. <http://dx.doi.org/10.1109/IGARSS.2014.6947113>.
- Duffour, C., Lagouarde, J.-P., Olioso, A., Demarty, J., Roujean, J.-L., 2015a. Driving factors of the directional variability of thermal infrared signal in temperate regions. *Remote Sens. Environ.* 177, 248–264. [doi.org/10.1016/j.rse.2016.02.024](http://dx.doi.org/10.1016/j.rse.2016.02.024).
- Duffour, C., Olioso, A., Demarty, J., Van der Tol, C., Lagouarde, J.-P., 2015b. An evaluation of SCOPE: a tool to simulate the directional anisotropy of satellite-measured surface temperatures. *Remote Sens. Environ.* 158, 362–375. <http://dx.doi.org/10.1016/j.rse.2014.10.019>.
- Farquhar, G.D., von Caemmerer, S., Berry, J.A., 1980. A biochemical model of photosynthetic CO_2 assimilation in leaves of C 3 species. *Planta* 149, 78–90. <http://dx.doi.org/10.1007/BF00386231>.
- Gastellu-Etchegorry, J.P., Martin, E., Gascon, F., 2004. DART: a 3D model for simulating satellite images and studying surface radiation budget. *Int. J. Remote Sens.* 25 (1), 73–96.
- Guillevic, P., Bork-Unkelbach, A., Goettsche, F.M., Hulley, G., Gastellu-Etchegorry, J.P., Olesen, F., Privette, J.L., 2013. Directional viewing effects on satellite land surface temperature products over sparse vegetation canopies - a multi-sensor analysis. *IEEE Geosci. Remote Sens. Lett.* - Spec. Str. on Biophys. Var. and Spat. Heterog. in Agric. Landsc. 10 (6), 1464–1468.
- Huang, H., Wang, L., Zhang, Y., Liu, Q., 2008. Temporal and spatial thermal radiation distribution analysis within and above crop canopies by 3D simulation. *Proc. 8th Int. Symp. on Spatial Accuracy Assessment in Natural Resources and Environmental Sciences*, pp. 313–320 Shanghai, P. R. China, June 25–27.
- Jacquemoud, S., Baret, F., 1990. PROSPECT: A model of leaf optical properties spectra. *Remote Sens. Environ.* 34, 75–91. [http://dx.doi.org/10.1016/0034-4257\(90\)90100-Z](http://dx.doi.org/10.1016/0034-4257(90)90100-Z).
- Jupp, D., 2000. A Compendium of Kernel & Other (Semi-) Empirical BRDF Models Doc. www.cossa.csiro.au/tasks/brdf, pp. 1–18.
- Kabsch, Olesen, F.S., Prata, F., 2008. Initial results of the land surface temperature (LST) validation with the Evora, Portugal ground-truth station measurements. *Int. J. Remote Sens.* 29 (17/18), 5329–5345.
- Kimes, D.S., Kirchner, J.A., 1983. Directional radiometric measurements of row-crop temperatures. *Int. J. Remote Sens.* 4, 299–311. <http://dx.doi.org/10.1080/01431168308948548>.
- Lagouarde, J.-P., Irvine, M., 2008. Directional anisotropy in thermal infrared measurements over Toulouse City centre during the CAPITOUL measurement campaigns: first results. *Meteorog. Atmos. Phys.* 102, 173–185. <http://dx.doi.org/10.1007/s00703-008-0325-4>.
- Lagouarde, J.-P., Ballans, H., Moreau, P., Guyon, D., Coraboeuf, D., 2000. Experimental study of brightness surface temperature angular variations of maritime pine (*Pinus pinaster*) stands. *Remote Sens. Environ.* 72, 17–34. [http://dx.doi.org/10.1016/S0034-4257\(99\)00085-1](http://dx.doi.org/10.1016/S0034-4257(99)00085-1).
- Lagouarde, J.-P., Hénon, A., Kurz, B., Moreau, P., Irvine, M., Voogt, J., Mestayer, P., 2010. Modelling daytime thermal infrared directional anisotropy over Toulouse City centre. *Remote Sens. Environ.* 114, 87–105. <http://dx.doi.org/10.1016/j.rse.2009.08.012>.
- Lagouarde, J.-P., Bach, M., Sobrino, J.A., Boulet, G., Briottet, X., Cherali, S., 2013. The MISTIGRI thermal infrared project: scientific objectives and mission specifications. *Int. Journal of Remote Sensing* 34 (9–10), 3437–3466. <http://dx.doi.org/10.1080/01431161.2012.716921>.
- Lagouarde, J.-P., Dayau, S., Moreau, P., Guyon, D., 2014. Directional anisotropy of brightness surface temperature over vineyards: case study over the Medoc Region (SW France). *IEEE Geosci. Remote Sens. Lett.* 11, 574–578. <http://dx.doi.org/10.1109/LGRS.2013.2282492>.
- Lagouarde, J.-P., Irvine, M., Dupont, S., 2015. Atmospheric turbulence induced errors on measurements of surface temperature from space. *Remote Sens. Environ.* 168, 40–53. <http://dx.doi.org/10.1016/j.rse.2015.06.018>.
- Masson, V., et al., 2008. The canopy and aerosol particles interactions in Toulouse urban layer (CAPITOUL) experiment. *Meteorog. Atmos. Phys.* 102, 135–157. <http://dx.doi.org/10.1007/s00703-008-0289-4>.

- Nelder, J.A., Mead, R., 1965. A simplex method for function minimization. *Comput. J.* 7, 308–313. <http://dx.doi.org/10.1093/comjnl/7.4.308>.
- Pinheiro, A.C.T., Privette, J.L., Guillevic, P., 2006. Modeling the observed angular anisotropy of land surface temperature in a Savanna. *IEEE Trans. Geosci. Remote Sens.* 44 (4), 1036–1047.
- Pires, A., Ermida, S., Trigo, I., 2015. *LST Merged Product*. Globtemp, Reading.
- Roujean, J.-L., 2000. A parametric hot spot model for optical remote sensing applications. *Remote Sens. Environ.* 71, 197–206. [http://dx.doi.org/10.1016/S0034-4257\(99\)00080-2](http://dx.doi.org/10.1016/S0034-4257(99)00080-2).
- Snyder, W.C., Wan, Z., 1998. BRDF models to predict spectral reflectance and emissivity in the thermal infrared. *IEEE Trans. Geosci. Remote Sens.* 36, 214–225. <http://dx.doi.org/10.1109/36.655331>.
- Su, L., Li, X., Friedl, M., Strahler, A., Gu, X., 2002. A kernel-driven model of effective directional emissivity for non-isothermal surfaces. *Prog. Nat. Sci.* 12, 603–607.
- Van der Tol, C., Verhoef, W., Timmermans, J., Verhoef, A., Su, Z., 2009. An integrated model of soil-canopy spectral radiances, photosynthesis, fluorescence, temperature and energy balance. *Biogeosciences* 6, 3109–3129. <http://dx.doi.org/10.5194/bg-6-3109-2009>.
- Verhoef, W., Jia, L., Xiao, Q., Su, Z., 2007. Unified optical-thermal four-stream radiative transfer theory for homogeneous vegetation canopies. *IEEE Trans. Geosci. Remote Sens.* 45, 1808–1822. <http://dx.doi.org/10.1109/TGRS.2007.895844>.
- Vermote, E., Justice, C.O., Breon, F.-M., 2009. Towards a generalized approach for correction of the BRDF effect in MODIS directional reflectances. *IEEE Trans. Geosci. Remote Sens.* 47, 898–908. <http://dx.doi.org/10.1109/TGRS.2008.2005977>.
- Vinnikov, K.Y., Yu, Y., Goldberg, M.D., Tarpley, D., Romanov, P., Laszlo, I., Chen, M., 2012. Angular anisotropy of satellite observations of land surface temperature. *Geophys. Res. Lett.* 39, L23802. <http://dx.doi.org/10.1029/2012GL054059>.
- Wallace, J., Verhoef, A., 2000. *Modelling interactions in mixed-plant communities: light, water and carbon dioxide*. *Leaf Development and Canopy Growth*, pp. 204–250.
- Wanner, W., Li, X., Strahler, A.H., 1995. On the derivation of kernels for kernel-driven models of bidirectional reflectance. *J. Geophys. Res.* 100, 21077. <http://dx.doi.org/10.1029/95JD02371>.